Strain-tunable quantum dot embedded in a nanowire antenna

PHYSICAL REVIEW B **90**, 201408(R) (2014)

Strain-tunable quantum dot embedded in a nanowire antenna

P. E. Kremer,[1,*] A. C. Dada,[1,*] P. Kumar,[1] Y. Ma,[1] S. Kumar,[1] E. Clarke,[2] and B. D. Gerardot[1,†]
[1]*Institute of Photonics and Quantum Sciences, SUPA, Heriot-Watt University, Edinburgh EH14 4AS, United Kingdom*
[2]*EPSRC National Centre for III-V Technologies, University of Sheffield, Sheffield S1 3JD, United Kingdom*
(Received 10 September 2014; revised manuscript received 5 November 2014; published 24 November 2014)

We demonstrate an elastically tunable self-assembled quantum dot in a nanowire antenna that emits single photons with resolution-limited spectral linewidths. The single-photon device is composed of a single quantum dot embedded in a top-down fabricated nanowire waveguide integrated onto a piezoelectric actuator. Nonresonant excitation leads to static (fluctuating) charges likely at the nanowire surface, causing DC Stark shifts (inhomogeneous broadening); for low excitation powers, the effects are not observed, and resolution-limited linewidths are obtained. Despite significant strain-field relaxation in the high-aspect-ratio nanowires, we achieve up to 1.2-meV tuning of a dot's transition energy. Single-photon sources with high brightness, resolution-limited linewidths, and wavelength tunability are promising for future quantum technologies.

DOI: 10.1103/PhysRevB.90.201408 PACS number(s): 85.35.Be, 78.55.Cr, 78.67.−n, 71.70.Fk

Self-assembled quantum dots (QDs) can generate indistinguishable photons [1–3], entangled photon pairs [4,5], and entangled spins and photons [6–8] due to the large oscillator strengths, clean selection rules, and relatively coherent spin states [9,10] of trapped carriers in QDs. To exploit these characteristics for linear-optical quantum computing [11,12] or quantum repeaters and distributed quantum networks [13,14], three crucial requirements of scalable QD devices are as follows: (i) efficient collection of the spontaneous emission into a single optical mode, (ii) minimal inhomogeneous broadening to enable transform-limited linewidths, and (iii) spectral tunability so that each dot can be made indistinguishable [15,16].

Multiple approaches to enhance the extraction efficiency (η), defined here as the ratio of power collected by an objective lens to the total power emitted from a dipole, have been pursued. A common strategy is to create a highly directional far-field radiation pattern, which has been achieved for QDs embedded in both high-Q cavities [17–19] and low-Q planar cavity structures [20–22]. Recently, subwavelength dielectric nanowires have been shown [23,24] to act as highly efficient waveguides with tailorable far-field radiation patterns [25–27]. Unlike high-Q cavities, these waveguides are compatible with large spectral tunability as the spontaneous emission is funneled into the waveguide over a wide spectral range with high fidelity. Hence, highly tunable and efficient quantum photonic devices can be envisioned with this platform.

Reversible *in situ* manipulation of single particles in QDs can best be achieved with electric [15,28–31] and strain [16,21,32–34] fields. Successful electrical contacting of QDs embedded in vertical nanowires [35] has yet to be demonstrated due to the difficulty of fabricating reliable nanoscale metal-semiconductor contacts. *In situ* strain tuning of nanowires also presents challenges not present for bulk structures as significant strain-field relaxation along the length of the nanowire occurs in high-aspect-ratio structures. Thus far, strain fields have been used to dynamically modulate [36–38] and quasipermanently control [39] the electronic properties of QDs in nanowire waveguides. However, to date, reversible *in situ* tuning of two-level emitters in nanowire waveguides has not been realized.

In addition to high η and pure single-photon emission, a requirement of single-photon emitters for some applications is transform-limited linewidths (Γ_{rad}). However, localized charges in the environment of the QD can shift a dot's emission energy via the quantum confined Stark effect [40]. Fluctuations in the microscopic charge distribution in the dot's environment can then lead to spectral fluctuations. The effect of spectral fluctuations is determined by the ratio $\hbar/\Gamma_{\mathrm{rad}}$ and the time scale of the charge fluctuation; the spectroscopic manifestation of the fluctuations is also determined by the experimental acquisition time [41,42]. In semiconductors, fluctuating charges are omnipresent, particularly at defects formed at interfaces [40] and free surfaces [43,44]. Therefore, QDs in small-diameter nanowires are particularly susceptible to significant spectral fluctuations [42,45,46].

Here we demonstrate an elastically tunable QD embedded in a nanowire waveguide which emits single photons with linewidths limited by our experimental resolution. We develop a deterministic top-down fabrication procedure to create nanowires with desired geometries. Nonresonant photoluminescence (PL) spectroscopy of QDs in these nanowires shows that the QD emission can be outcoupled with high fidelity, although with less-than-ideal success rates. Statistics from the characterization of 40 QDs in 16 nominally identical nanowires yield $\bar{\eta} = 13\% \pm 10\%$ with a maximum $\eta_{\mathrm{max}} = 57\%$. The large variation in η is ascribed to variations in the radial positions of the QDs as well as surface roughness and asymmetry in the nanowire structures. At low excitation powers, resolution-limited spectral linewidths are found for some QDs. At higher excitation powers, DC Stark shifts and inhomogeneous linewidth broadening are observed due to static and fluctuating electric fields (F and δF, respectively) at the QD position, respectively. We quantitatively estimate F and δF at the QD position by assuming they are generated by filling of nearby nanowire surface states via above-band-gap excitation. The resolution-limited linewidths at low excitation powers lead to optimism that resonant driving of the QDs

*These authors contributed equally to this work.
†b.d.gerardot@hw.ac.uk

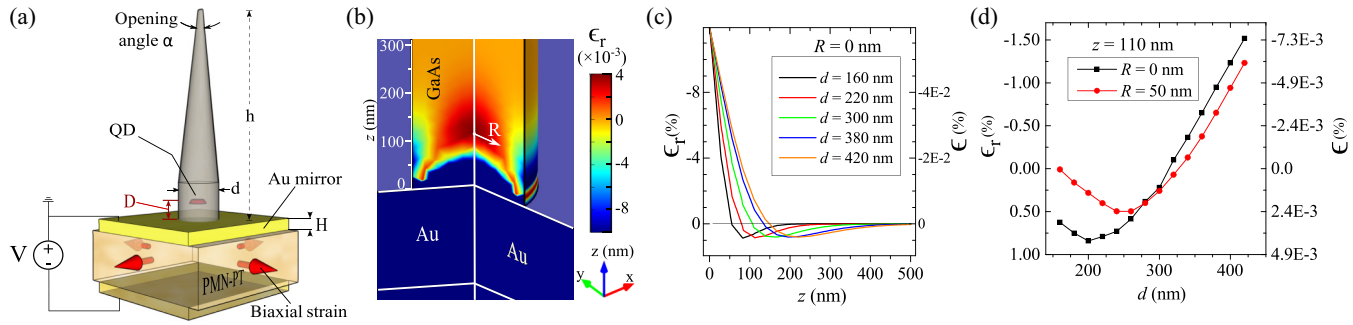

FIG. 1. (Color online) (a) Sketch showing the geometry of our device where D is the distance between the quantum dot and the Au mirror, d is the diameter of the pillar at the quantum dot position, h is the height of the pillar, and α is the opening angle of the pillar taper. The lead magnesium niobate lead titanate (PMN-PT) crystal has electrical gold contacts (with thickness H) on both sides for voltage tuning. The top Au contact also acts as a bonding layer and mirror for the broadband optical antenna. (b) Simulation of strain relaxation in the nanowire using the finite-element method (FEM). The plot shows the profile of relative strain $\varepsilon_r = \varepsilon(x,y,z)/|\varepsilon_0|$ where the strain is $\varepsilon(x,y,z)$ and the strain in the PMN-PT crystal is ε_0. The color legend is scaled to highlight the strain-field relaxation within the nanowire. (c) Plot of the strain ε and relative strain ε_r as a function of the distance along the z axis from the Au/GaAs interface ($z = 0$ nm at a radially centered position $R = 0$ nm). (d) Plot of ε and ε_r at $z = 110$ and $R = 0{,}50$ nm. The nanowire diameter $d = 220$ nm in (b), and $\varepsilon_0 = -0.1\%$ in (b)–(d).

could be successfully achieved in future experiments for full quantum-optical control of the QD. Such experiments are greatly assisted by *in situ* tuning of the QD excitonic transition energy [29], which we demonstrate here with nanowire QDs via bonding to a piezoelectric crystal. Statistics from excitonic transitions in 30 QDs shows reversible energy-tuning amplitudes (δE) of $\overline{\delta E} = 0.40 \pm 0.33$ meV (based on tuning-slopes statistics and an applied piezovoltage of 1 kV) and a maximum amplitude $\delta E_{\max} = 1.2$ meV with small hysteresis effects. The active strain tuning could enable the reduction of the neutral exciton fine-structure splitting [21,32,34] for the generation of entangled-photon pairs from high-quality self-assembled InGaAs QDs in GaAs nanowires, similar to what has recently been achieved with QDs with nominally small fine-structure splittings in InP nanowires [47,48].

The design criteria to optimize both the coupling of the QD emission into the fundamental mode of a nanowire waveguide and the directionality of the far-field radiation are well established [25–27]. A *reduced nanowire diameter* (d/λ) of 0.235 is found to optimally funnel the QD emission into the fundamental HE_{11} mode in both directions along a GaAs nanowire. A mirror terminates one end of the nanowire to reflect incident light towards the out-coupling nanowire end where a conical taper is introduced to adiabatically expand the confined mode into a plane wave in free space. The angle of the conical tapering (α) determines both the reflection of the guided mode and the divergence angle of the far-field radiation pattern; for a QD located at the nanowire center, $\alpha < 10^\circ$ leads to $\eta > 50\%$ (see Sec. SII in the Supplemental Material [49]). Coupling of the light to the fundamental mode is optimized by placing the dot at the electric field's antinode caused by the standing-wave pattern between the mirror and the emitter. An idealized sketch of our device is shown in Fig. 1(a). It consists of a self-assembled QD located a distance D from a Au mirror and radially centered in a nanowire with height h, diameter d, and taper angle α. The Au mirror (with thickness $H = 200$ nm) is deposited directly onto a single-crystal PMN-PT substrate (300-μm thick) to also act as an electrical contact for piezoelectric biaxial strain tuning. This top electrical contact is grounded to prevent large electric fields near the QD. The complete fabrication procedure is detailed in the Supplemental Material [49].

To better understand the challenge associated with strain tuning a QD in a high-aspect-ratio nanowire, we have simulated the complete device using FEM [Figs. 1(b)–1(d)]. We quantify strain-field relaxation by means of the *relative strain* (ε_r), defined as $\varepsilon_r = \varepsilon(x,y,z)/|\varepsilon_0|$, where $\varepsilon(x,y,z)$ is the strain at a given position with coordinates (x,y,z) and ε_0 is the strain in the PMN-PT crystal. Figure 1(b) shows the profile of relative strain ε_r with $\varepsilon_0 = -0.1\%$ and $d = 220$ nm. The color legend is scaled to highlight the strain-field relaxation within the nanowire. In Fig. 1(c), we show the plot of ε_r (and ε) as a function of axial position along the nanowire for different diameters d at the center of the nanowire $R = 0$ nm. For $D = 110$ nm, we also show the strain as a function of d for radial positions $R = 0{,}50$ nm in Fig. 1(d). The modeling first confirmed that the strain relaxation is linear with respect to the applied strain, i.e., $\varepsilon_r \propto \varepsilon_0$, for $\varepsilon_0 = -0.05\%, \ldots, -0.5\%$ (which is within the range expected for a PMN-PT single crystal for an applied voltage of 0 to 1 kV [50,51]). The model shows that the strain field generated by the piezoelectric crystal relaxes substantially ($\approx$80%) across the 200-nm-thick Au layer. We note that, although the inclusion of a silica spacer between the nanowire and the Au layer has been shown to increase modal reflectivity [25,27], its absence in our device enhances strain transfer to the nanowire from the Au layer by $\approx$20% based on our simulation results. The remaining strain field transmitted across the Au/GaAs interface is highly dependent on the diameter of the nanowire as well as on the radial and axial positions within the nanowire. In particular, we see increased relaxation with reducing nanowire diameter [Fig. 1(c)] as well as higher strain fields nearer the center of the nanowire [Fig. 1(d)]. Although the applied strain is compressive, regions of tensile strain are seen as the strain relaxes along the nanowire. The axial position for optimal strain tuning is found to be in conflict with that required for optimal coupling to the HE_{11} mode. In fact, with geometry optimized for coupling at $\lambda = 950$ nm (i.e., $D = 80$, $d = 220$,

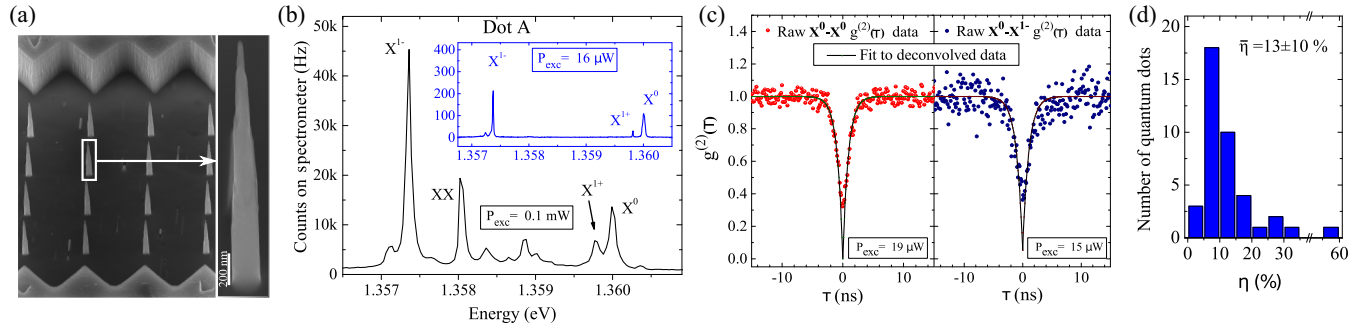

FIG. 2. (Color online) (a) SEM image of an array of nominally identical tapered nanowires with $d = 232 \pm 4$, $D = 110$ nm, $h = 2$ μm, and $\alpha = 9.8 \pm 1.3^\circ$. The enlarged image is of the nanowire from which the spectrum in (b) is obtained. Unetched areas forming μ structures ($\approx 3 \times 7$ μm^2 in area) are partly visible on the top and bottom edges of the nanowire array. (b) The PL spectrum from dot A at saturation power with an estimated extraction efficiency of $\eta = 25.9\%$. The inset shows a spectrum from the same dot below saturation. (c) Autocorrelation of X^{1-} and cross correlation between X^{1-} and X^0 for dot B obtained at an excitation power of 19 μW. (d) A histogram of the estimated extraction efficiencies η from QDs in the 16 nanowires shown in (a).

and $R = 0$ nm), we obtain $\varepsilon_r = 0.04\%$. Although changing to $D < 80$ nm significantly increases ε_r, it will likely lead to increased spectral fluctuations due to the effect of surface states at the mirror/nanowire interface [40,43]. Keeping $d = 220$ and $R = 0$ nm for $D > 80$ nm, ε_r is maximized at $D \approx 110$ nm before completely relaxing by $D = 250$ nm. For a QD at $R = 0$ and $D = 110$ nm in a pillar with diameter $d = 220$ nm, the model predicts a relative strain of $\varepsilon_r = 0.8\%$ whereas η is only moderately affected (see Supplemental Material [49]), demonstrating the validity of the device as an efficient and elastically tunable platform for quantum photonics.

We have spectroscopically characterized numerous nanowires with constant D (110 nm) and h (2 μm) but varying d and α. Although the nanowires are not deterministically aligned to the randomly positioned QDs, the wafer has a suitably high QD density ($\sim 1.2 \times 10^{10}$ cm^{-2}) for us to typically observe three to five spectrally isolated QDs per nanowire. A scanning-electron-microscope (SEM) image of an array of some of the brightest devices is shown in Fig. 2(a), where $d = 223$ nm (corresponding to $0.227 < d/\lambda < 0.235$ for 920 nm $< \lambda <$ 950 nm, the typical range of ground-state exciton emission wavelengths for the QDs in this wafer) and $\alpha \approx 10^\circ$.

PL spectra were acquired from the sample at $T = 4.5$ K using a confocal microscope with a 0.82 numerical-aperture objective lens. The QDs were excited nonresonantly ($\lambda_{\text{exc}} =$ 830 nm) using a continuous-wave laser diode. To maximize the PL signal we focused the collection optics at the top of the nanowire while the excitation laser was focused at the bottom of the nanowire. The PL was characterized using a spectrometer (0.5-m focal length and 1800-grooves mm^{-1} grating giving a resolution of $\Gamma_{\text{spect}} = 35$ μeV (full width at half maximum) measured using a narrow-band laser) and a liquid-nitrogen-cooled Si charge-coupled-device (CCD) camera. Second-order correlation measurements were acquired using a Hanbury-Brown-Twiss setup (350-μeV spectral resolution) with two silicon single-photon avalanche diodes (timing jitter $\approx$500 ps) and timing electronics.

The PL spectra from a QD (dot A) found in one of the brightest wires is shown in Fig. 2(b). The exciton states are identified by the characteristic Coulomb interactions observed in experiments with similar QDs in charge-tunable devices [52] and the linear (quadratic) power dependence for single (bi-) excitons. The spectra in Fig. 2(b) are representative of what we typically observe from QDs in the nanowires, except with varying central energies and peak intensities. Further confirmation of the state assignment can be obtained by measuring the photon-intensity correlations between separate excitonic states [53]. Figure 2(c) shows the second-order autocorrelation measurement of the X^{1-} state from another QD, dot B. The raw data show $g^2(0) < 0.5$ whereas the fit to data deconvolved for detector jitter shows $g^2(0) \approx 0$, signifying high-purity single-photon emission. The second-order cross-correlation measurement between the X^0 and the X^{1-} states [Fig. 2(d)] also demonstrates clear antibunching, signifying that these states originate from the same QD [54]. Also, the absence of complex dynamics in the second-order correlation experiments demonstrates charge-state stability on short time scales [44,55].

The correct excitonic line assignment enables estimation of the total η from a single dot, defined as the power collected into the objective lens divided by the power emitted by the QD. The latter can be estimated at saturation from the emission rates of each excitonic state (defined as the inverse of the transition's lifetime) and the relative integrated intensities of each excitonic state. The efficiency of the experimental setup (from the objective lens to the CCD camera) was calibrated using a tunable laser at the QD emission wavelength. η was thus estimated for the 40 brightest dots in the 16 nominally identical nanowires as summarized in the histogram in Fig. 2(d). We find $\eta_{\text{max}} = 57\%$ for our brightest dot when each excitonic state is included, and $\bar{\eta} = 13\% \pm 10\%$. The most obvious explanation for the large standard deviation of η is the random positioning of the dots radially in the nanowires, which could be remedied in the future with a deterministic positioning technique [18]. Additionally, the SEM images reveal surface defects and slight asymmetry in the nanowires, which may adversely affect performance. However, we are unable to correlate differences in particular structures with their brightness. Curiously, we have spectroscopically characterized

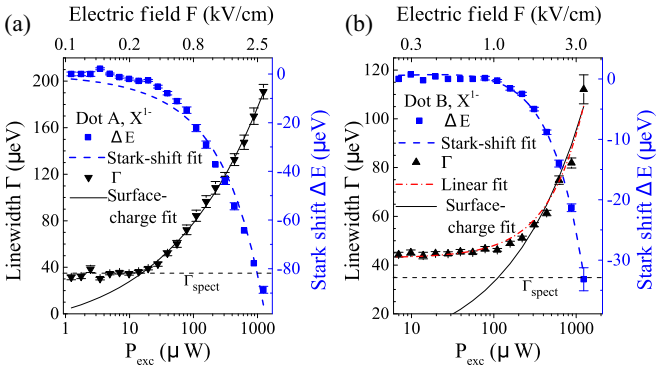

FIG. 3. (Color online) The measured spectral linewidths (Γ) and Stark shifts (ΔE) as a function of excitation power (P_{exc}) are shown for the X^{1-} line for dot A and dot B in (a) and (b), respectively. A fit of the Stark effect allows an estimated electric field (F) to be calculated in each case. For dot A, the *surface-charge fit* used to describe the dependence of Γ on P_{exc} is based on a fluctuating δF estimated from the electronic shot noise of the static F. For dot B, the *surface-charge fit* fails to match the data as Γ exhibits a linear dependence to P_{exc}.

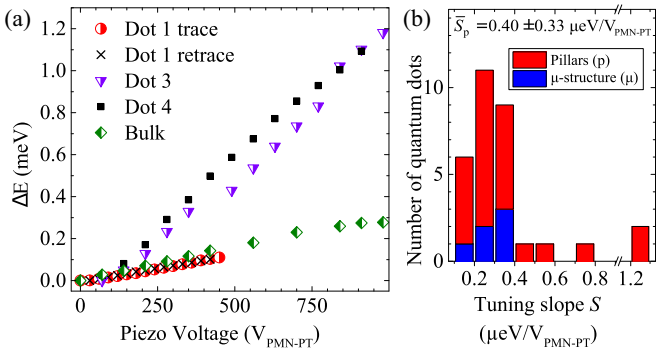

FIG. 4. (Color online) (a) Strain tuning the energies of different single QD excitons. Each QD in each pillar exhibits a different strain-tuning slope ($S = \Delta E/\Delta V_{\text{PMN-PT}}$) as shown in the histogram in (b). Also shown in the histogram are tuning slopes S_μ for QDs in the μ-structure membrane ($S_\mu = 0.29 \pm 0.06\ \mu\text{eV/V}_{\text{PMN-PT}}$).

numerous nanowire structures made from the same wafer with smoother features and better symmetry but worse η.

Nonresonant PL spectroscopy enables investigation of the effect of the nearby nanowire surfaces on the spectral linewidths and exciton energies of QDs. The nonresonant laser excites carriers above the GaAs band gap that can relax into the QD as well as fill defect surface states; increasing the excitation power (P_{exc}) increases the number of carriers at the nanowire surface. For the self-assembled InGaAs QDs investigated here, $\Gamma_{\text{rad}} \sim 1\ \mu$eV. Figures 3(a) and 3(b) show the energy detuning (ΔE) and measured linewidths (Γ) for the X^{1-} for dots A and B, respectively. For $P_{\text{exc}} \leqslant 20\ \mu$W for dot A, ΔE is zero, and Γ is resolution limited. For dot B, ΔE is zero, and Γ is constant ($\sim$45 μeV) but inhomogeneously broadened above the experimental resolution limit in the low-power regime ($P_{\text{exc}} \leqslant 100\ \mu$W). For both QDs, as P_{exc} increases from the low-power regime, ΔE increases, and Γ broadens without saturation. To better understand and quantify the effect of the surface states, we exploit the ability of the QD itself to function as an *in situ* probe of the local electric field [30,31,40,56]. In an electric field, the quantum dot dipole manifests a Stark shift with quadratic field dependence, and the energy detuning is given by $\Delta E = -pF + \beta F^2$, where F is the electric field, p is the permanent dipole moment, and β is the polarizability. To gain physical insight, we express $p = er$, where e is the electronic charge and r is the electron-hole wave-function separation.

To estimate F at the position of the QD based on ΔE observed in PL measurements, we assume $\beta = -4\ \mu\text{eV}\,(\text{kV}^{-1}\,\text{cm}^{-1})^2$ [30,31]. The fits from this procedure give $r = 2.3 \pm 0.6$ and -0.34 ± 0.02 Å for dots A and B, respectively. The fits are shown as the dashed lines in Fig. 3 with the extracted values for F shown on the top x axis in the figures. The fits agree well with the data, and we observe that F is linearly proportional to $\sqrt{P_{\text{exc}}}$ for each QD. Furthermore, we can estimate the fluctuating electric field δF by assuming the fluctuation (δn) in the number of electrons (n) located at the surface is proportional to the electronic shot noise: $\delta n \propto \sqrt{n}$. We calculate n by assuming electrons a distance $d/2$ create F and then use δF to find the corresponding $\delta(\Delta E) \equiv \Gamma$ from the Stark equation. For dot A, the estimated power broadening of Γ [shown as the solid line labeled *surface-charge fit* in Fig. 3(a)] fits the experimental data very well above the system's resolution limit. The surface-charge fit also enables us to estimate the power broadening below the resolution limit. Both the data and the extrapolated fit suggest the inhomogeneous broadening is dominated by the charges generated by the excitation laser at the nanowire surface. The results from dot A are promising for the generation of indistinguishable photons from a QD in a nanowire antenna. On the other hand, a fit with a linear dependence of Γ on P_{exc} is found to fit the data for dot B much better than a surface-charge fit, even in the high P_{exc} regime. This result suggests that unlike the behavior of dot A's power broadening, dot B's linewidth broadening is not solely caused by the charge fluctuations generated at the nanowire surface by nonresonant excitation.

Finally, we demonstrate the elastic tunability of the exciton states. Figure 4(a) shows examples of exciton detuning for QDs in different nanowire antennas as a function of applied bias to the piezoelectric crystal ($V_{\text{PMN-PT}}$). We observe varied strain-tuning slopes for each QD in each nanowire as summarized for 30 QDs in the histogram in Fig. 4(b). Also shown is a histogram of the strain tuning of QDs located in the roughly $3 \times 7\ \mu\text{m}^2$ unetched region of the sample nearby the nanowires (μ-structure membrane). This is partly visible in Fig. 2(a) on the top and bottom edges of the array. In general, the strain tuning is achieved with small amounts of hysteresis as shown for Dot 1. A maximum tuning amplitude of $\delta E \approx 1.2$ meV was achieved in the experiment. The large standard deviation in tuning is expected for two reasons: (i) The amplitude and even sign of the strain field are highly dependent on the radial position of the QD in the nanowire (as shown in Fig. 1); and (ii) strain tuning of the quantum states is highly dependent on the exact morphology of the dot, which is unique for every QD [33,34,57]. Despite the significant strain-field relaxation in the Au contact and the nanowire, we achieve substantial *in situ* strain tuning of the QD excitonic transition energies. Further

improvement in the tuning range can be obtained by reducing the Au-layer thickness H and moving the QD closer to the mirror, which may however lead to more spectral fluctuations.

In conclusion, we have demonstrated an elastically tunable QD embedded in a nanowire waveguide emitting single photons with resolution-limited linewidths. The device enables strain tuning of excitons by up to 1.2 meV, which could enable resonant fluorescence experiments, reduction in fine-structure splitting for entangled photon-pair generation, and two-photon interference from separate QDs in nanowire antennas.

The authors would like to thank G. C. Ballesteros for assistance with the FEM software (COMSOL) and acknowledge the financial support for this work from a Royal Society University Research Fellowship, the EPSRC (Grants No. EP/I023186/1 and No. EP/K015338/1), and an ERC Starting Grant (Grant No. 307392).

[1] C. Santori, D. Fattal, J. Vučković, G. S. Solomon, and Y. Yamamoto, Nature (London) **419**, 594 (2002).
[2] S. Ates, S. M. Ulrich, S. Reitzenstein, A. Löffler, A. Forchel, and P. Michler, Phys. Rev. Lett. **103**, 167402 (2009).
[3] Y.-M. He, Y. He, Y.-J. Wei, D. Wu, M. Atatüre, C. Schneider, S. Höfling, M. Kamp, C.-Y. Lu, and J.-W. Pan, Nat. Nanotechnol. **8**, 213 (2013).
[4] N. Akopian, N. H. Lindner, E. Poem, Y. Berlatzky, J. Avron, D. Gershoni, B. D. Gerardot, and P. M. Petroff, Phys. Rev. Lett. **96**, 130501 (2006).
[5] C. Salter, R. Stevenson, I. Farrer, C. Nicoll, D. Ritchie, and A. Shields, Nature (London) **465**, 594 (2010).
[6] K. De Greve, P. L. McMahon, L. Yu, J. S. Pelc, C. Jones, C. M. Natarajan, N. Y. Kim, E. Abe, S. Maier, C. Schneider, M. Kamp, S. Höfling, R. H. Hadfield, A. Forchel, M. M. Fejer, and Y. Yamamoto, Nat. Commun. **4**, 2228 (2013).
[7] W. Gao, P. Fallahi, E. Togan, J. Miguel-Sanchez, and A. Imamoglu, Nature (London) **491**, 426 (2012).
[8] J. R. Schaibley, A. P. Burgers, G. A. McCracken, L.-M. Duan, P. R. Berman, D. G. Steel, A. S. Bracker, D. Gammon, and L. J. Sham, Phys. Rev. Lett. **110**, 167401 (2013).
[9] D. Press, T. D. Ladd, B. Zhang, and Y. Yamamoto, Nature (London) **456**, 218 (2008).
[10] D. Brunner, B. D. Gerardot, P. A. Dalgarno, G. Wüst, K. Karrai, N. G. Stoltz, P. M. Petroff, and R. J. Warburton, Science **325**, 70 (2009).
[11] E. Knill, R. Laflamme, and G. J. Milburn, Nature (London) **409**, 46 (2001).
[12] P. Kok and B. W. Lovett, *Introduction to Optical Quantum Information Processing*, 1st ed. (Cambridge University Press, Cambridge, UK, 2010).
[13] H. Kimble, Nature (London) **453**, 1023 (2008).
[14] N. Sangouard, C. Simon, H. de Riedmatten, and N. Gisin, Rev. Mod. Phys. **83**, 33 (2011).
[15] R. B. Patel, A. J. Bennett, I. Farrer, C. A. Nicoll, D. A. Ritchie, and A. J. Shields, Nat. Photonics **4**, 632 (2010).
[16] E. B. Flagg, A. Muller, S. V. Polyakov, A. Ling, A. Migdall, and G. S. Solomon, Phys. Rev. Lett. **104**, 137401 (2010).
[17] S. Strauf, N. G. Stoltz, M. T. Rakher, L. A. Coldren, P. M. Petroff, and D. Bouwmeester, Nat. Photonics **1**, 704 (2007).
[18] O. Gazzano, S. M. de Vasconcellos, C. Arnold, A. Nowak, E. Galopin, I. Sagnes, L. Lanco, A. Lemaître, and P. Senellart, Nat. Commun. **4**, 1425 (2013).
[19] K. H. Madsen, S. Ates, J. Liu, A. Javadi, S. M. Albrecht, I. Yeo, S. Stobbe, and P. Lodahl, Phys. Rev. B **90**, 155303 (2014).
[20] M. Davanço, M. Rakher, D. Schuh, A. Badolato, and K. Srinivasan, Appl. Phys. Lett. **99**, 041102 (2011).
[21] R. Trotta, P. Atkinson, J. Plumhof, E. Zallo, R. Rezaev, S. Kumar, S. Baunack, J. Schroeter, A. Rastelli, and O. Schmidt, Adv. Mater. **24**, 2668 (2012).
[22] Y. Ma, P. E. Kremer, and B. D. Gerardot, J. Appl. Phys. **115**, 023106 (2014).
[23] J. Claudon, J. Bleuse, N. S. Malik, M. Bazin, P. Jaffrennou, N. Gregersen, C. Sauvan, P. Lalanne, and J.-M. Gérard, Nat. Photonics **4**, 174 (2010).
[24] M. E. Reimer, G. Bulgarini, N. Akopian, M. Hocevar, M. B. Bavinck, M. A. Verheijen, E. P. Bakkers, L. P. Kouwenhoven, and V. Zwiller, Nat. Commun. **3**, 737 (2012).
[25] N. Gregersen, T. R. Nielsen, J. Claudon, J.-M. Gérard, and J. Mørk, Opt. Lett. **33**, 1693 (2008).
[26] I. Friedler, C. Sauvan, J.-P. Hugonin, P. Lalanne, J. Claudon, and J.-M. Gérard, Opt. Express **17**, 2095 (2009).
[27] J. Claudon, N. Gregersen, P. Lalanne, and J.-M. Gérard, ChemPhysChem **14**, 2393 (2013).
[28] J. J. Finley, P. W. Fry, A. D. Ashmore, A. Lemaître, A. I. Tartakovskii, R. Oulton, D. J. Mowbray, M. S. Skolnick, M. Hopkinson, P. D. Buckle, and P. A. Maksym, Phys. Rev. B **63**, 161305 (2001).
[29] A. Högele, S. Seidl, M. Kroner, K. Karrai, R. J. Warburton, B. D. Gerardot, and P. M. Petroff, Phys. Rev. Lett. **93**, 217401 (2004).
[30] B. D. Gerardot, S. Seidl, P. A. Dalgarno, R. J. Warburton, D. Granados, J. M. Garcia, K. Kowalik, O. Krebs, K. Karrai, A. Badolato, and P. M. Petroff, Appl. Phys. Lett. **90**, 041101 (2007).
[31] M. Vogel, S. Ulrich, R. Hafenbrak, P. Michler, L. Wang, A. Rastelli, and O. Schmidt, Appl. Phys. Lett. **91**, 051904 (2007).
[32] S. Seidl, M. Kroner, A. Högele, K. Karrai, R. J. Warburton, A. Badolato, and P. M. Petroff, Appl. Phys. Lett. **88**, 203113 (2006).
[33] C. E. Kuklewicz, R. N. Malein, P. M. Petroff, and B. D. Gerardot, Nano Lett. **12**, 3761 (2012).
[34] L. Sapienza, R. N. E. Malein, C. E. Kuklewicz, P. E. Kremer, K. Srinivasan, A. Griffiths, E. Clarke, M. Gong, R. J. Warburton, and B. D. Gerardot, Phys. Rev. B **88**, 155330 (2013).
[35] N. Gregersen, T. R. Nielsen, J. Mørk, J. Claudon, and J.-M. Gérard, Opt. Express **18**, 21204 (2010).
[36] I. Yeo, P.-L. de Assis, A. Gloppe, E. Dupont-Ferrier, P. Verlot, N. S. Malik, E. Dupuy, J. Claudon, J.-M. Gérard, A. Auffèves, G. Nogues, S. Seidelin, J.-Ph. Poizat, O. Arcizet, and M. Richard, Nat. Nanotechnol. **9**, 106 (2014).

[37] M. Montinaro, G. Wüst, M. Munsch, Y. Fontana, E. Russo-Averchi, M. Heiss, A. Fontcuberta i Morral, R. J. Warburton, and M. Poggio, Nano Lett. **14**, 4454 (2014).

[38] M. Weiß, J. B. Kinzel, F. J. Schlein, M. Heigl, D. Rudolph, S. Morkötter, M. Döblinger, M. Bichler, G. Abstreiter, J. J. Finley *et al.*, Nano Lett. **14**, 2256 (2014).

[39] M. Bouwes Bavinck, M. Zielinski, B. J. Witek, T. Zehender, E. P. Bakkers, and V. Zwiller, Nano Lett. **12**, 6206 (2012).

[40] J. Houel, A. V. Kuhlmann, L. Greuter, F. Xue, M. Poggio, B. D. Gerardot, P. A. Dalgarno, A. Badolato, P. M. Petroff, A. Ludwig, D. Reuter, A. D. Wieck, and R. J. Warburton, Phys. Rev. Lett. **108**, 107401 (2012).

[41] A. Berthelot, I. Favero, G. Cassabois, C. Voisin, C. Delalande, P. Roussignol, R. Ferreira, and J.-M. Gérard, Nat. Phys. **2**, 759 (2006).

[42] S. Bounouar, A. Trichet, M. Elouneg-Jamroz, R. André, E. Bellet-Amalric, C. Bougerol, M. Den Hertog, K. Kheng, S. Tatarenko, and J.-P. Poizat, Phys. Rev. B **86**, 085325 (2012).

[43] C. Wang, A. Badolato, I. Wilson-Rae, P. Petroff, E. Hu, J. Urayama, and A. Imamoğlu, Appl. Phys. Lett. **85**, 3423 (2004).

[44] M. Davanço, C. S. Hellberg, S. Ates, A. Badolato, and K. Srinivasan, Phys. Rev. B **89**, 161303(R) (2014).

[45] I. Yeo, N. S. Malik, M. Munsch, E. Dupuy, J. Bleuse, Y. M. Niquet, J. M. Gérard, J. Claudon, E. Wagner, S. Seidelin, A. Auffèves, J. P. Poizat, and G. Nogues, Appl. Phys. Lett. **99**, 233106 (2011).

[46] M. E. Reimer, G. Bulgarini, R. W. Heeres, B. J. Witek, M. A. M. Versteegh, D. Dalacu, J. Lapointe, P. J. Poole, and V. Zwiller, arXiv:1407.2833.

[47] T. Huber, A. Predojević, M. Khoshnegar, D. Dalacu, P. J. Poole, H. Majedi, and G. Weihs, arXiv:1405.3765.

[48] M. A. Versteegh, M. E. Reimer, K. D. Jöns, D. Dalacu, P. J. Poole, A. Gulinatti, A. Giudice, and V. Zwiller, Nat. Commun. **5**, 5298 (2014).

[49] See Supplemental Material at http://link.aps.org/supplemental/10.1103/PhysRevB.90.201408 for details on the fabrication procedure, determination of the experimental photon extraction efficiency, as well as finite-difference time-domain simulation of the structure.

[50] A. Herklotz, J. D. Plumhof, A. Rastelli, O. G. Schmidt, L. Schultz, and K. Dorr, J. Appl. Phys. **108**, 094101 (2010).

[51] S. Kumar, R. Trotta, E. Zallo, J. Plumhof, P. Atkinson, A. Rastelli, and O. Schmidt, Appl. Phys. Lett. **99**, 161118 (2011).

[52] P. A. Dalgarno, J. M. Smith, J. McFarlane, B. D. Gerardot, K. Karrai, A. Badolato, P. M. Petroff, and R. J. Warburton, Phys. Rev. B **77**, 245311 (2008).

[53] D. V. Regelman, U. Mizrahi, D. Gershoni, E. Ehrenfreund, W. V. Schoenfeld, and P. M. Petroff, Phys. Rev. Lett. **87**, 257401 (2001).

[54] B. D. Gerardot, S. Strauf, M. J. A. de Dood, A. M. Bychkov, A. Badolato, K. Hennessy, E. L. Hu, D. Bouwmeester, and P. M. Petroff, Phys. Rev. Lett. **95**, 137403 (2005).

[55] C. Santori, D. Fattal, J. Vučković, G. S. Solomon, E. Waks, and Y. Yamamoto, Phys. Rev. B **69**, 205324 (2004).

[56] A. N. Vamivakas, Y. Zhao, S. Fält, A. Badolato, J. M. Taylor, and M. Atatüre, Phys. Rev. Lett. **107**, 166802 (2011).

[57] K. D. Jöns, R. Hafenbrak, R. Singh, F. Ding, J. D. Plumhof, A. Rastelli, O. G. Schmidt, G. Bester, and P. Michler, Phys. Rev. Lett. **107**, 217402 (2011).